ACSNANO

www.acsnano.org

ARTICLE

Direct Detection of Conserved Viral Sequences and Other Nucleic Acid Motifs with Solid-State Nanopores

Komal Sethi, Gabrielle P. Dailey, Osama K. Zahid, Ethan W. Taylor, Jan A. Ruzicka, and Adam R. Hall*

Cite This: https://doi.org/10.1021/acsnano.0c10887

Read Online

ACCESS | Metrics & More | Article Recommendations | Supporting Information

ABSTRACT: The rapid and reliable recognition of nucleic acid sequences is essential to a broad range of fields including genotyping, gene expression analysis, and pathogen screening. For viral detection in particular, the capability is critical for optimal therapeutic response and preventing disease transmission. Here, we report an approach for detecting identifying sequence motifs within genome-scale single-strand DNA and RNA based on solid-state nanopores. By designing DNA oligonucleotide probes with complementarity to target sequences within a target genome, we establish a protocol to yield affinity-tagged duplex molecules the same length as the probe only if the target is present. The product can subsequently be bound to a protein chaperone and analyzed quantitatively with a selective solid-state nanopore assay. We first use a model DNA genome (M13mp18) to validate the approach, showing the successful isolation and detection of multiple target sequences simultaneously. We then demonstrate the protocol for the detection of RNA viruses by identifying and targeting a highly conserved sequence within human immunodeficiency virus (HIV-1B).

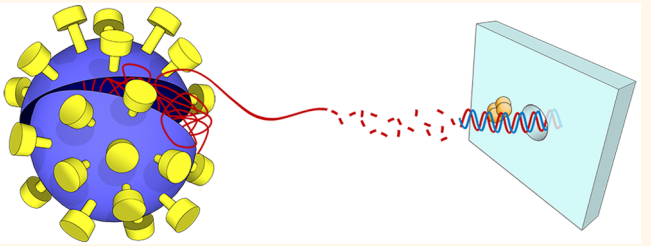

KEYWORDS: *solid-state nanopore, viral detection, biomarkers, DNA, RNA, HIV*

INTRODUCTION

Viruses are nanoscopic particles containing genetic material that must invade living organisms and take over their cellular machinery to replicate. In support of this mechanism, they can be both highly transmissible and rapidly mutating, enabling them to evolve quickly. From the identification of Yellow Fever virus as the first reported[1] human virus in 1900, viruses have been a consistent threat to human health. Indeed, three to four new species of human virus are identified every year[2,3] accounting for over two-thirds of new human pathogens.[4] In recent history, diverse diseases have emerged from viral vectors including human immunodeficiency virus (HIV), Ebola, avian influenza, Zika, and middle east respiratory syndrome (MERS).[5,6] Enhanced global movement has further exacerbated the problem of rampant transmission, increasing the likelihood of global pandemics like the one caused[7] by SARS-CoV-2 beginning in 2019.

Viral detection capabilities are critical for combating the spread of such diseases, providing both accurate diagnosis for early treatment planning and a means of performing contact tracing for containment.[6] While a broad range of diagnostic approaches exist for this purpose, current technologies still encounter significant challenges. For example, tests incorporating polymerase chain reaction (PCR)—including quantitative PCR (qPCR) and reverse transcription PCR (RT-PCR)—are considered gold standards in viral diagnostics.[6,8] While these techniques are highly sensitive, they can also feature a risk of contamination and bias,[9−11] commonly rely on expensive optical systems for analysis, and are often slow. Indeed, the typical hours-long cycling necessary for most PCR assays is a critical factor limiting throughput and increasing time-to-answer. Alternatively, immunoassays are also used extensively to identify protein markers associated with viral exposure. While high sensitivity can be achievable through several measurement modalities including fluorescence,[12] radiolabeling,[13] and colorimetric (biochemical),[14] immunodetection also relies on expensive reagents and can suffer from cross reactivity, resulting in false negatives or false positives.[15] Finally, recent developments have been made in the application of next-generation sequencing (NGS)[6] and mass

Received: December 29, 2020
Accepted: April 26, 2021

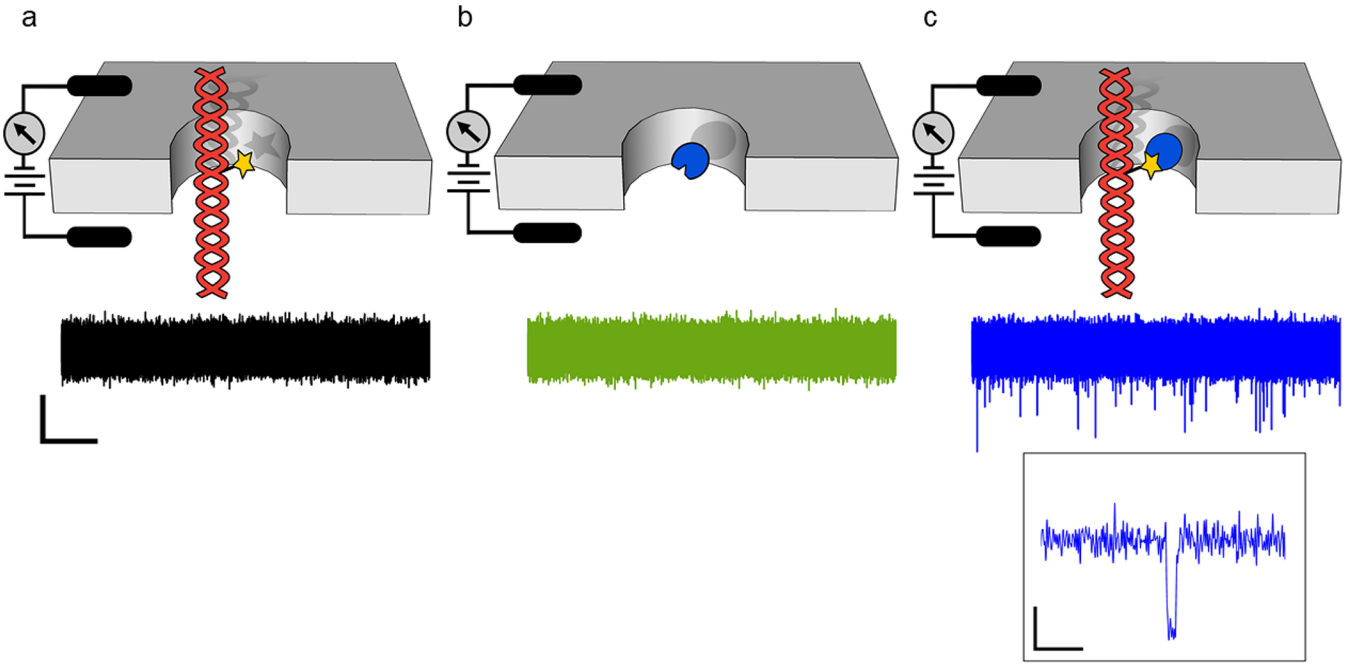

Figure 1. Selective solid-state nanopore assay. Diagrammatic representation (top) and example current trace (bottom) for the translocation of (a) biotinylated duplex nucleic acids alone, (b) monovalent streptavidin protein alone, and (c) duplex nucleic acids bound to monovalent streptavidin. The scale bars for all three current traces represent 500 pA (vertical) and 250 ms (horizontal). Individual components transit through the nanopore rapidly and yield no events, while nucleoprotein complexes result in an event cascade due to steric hindrance. A 60 bp duplex DNA construct was used for these measurements, and all traces were recorded at 300 mV applied bias. Inset: magnified view of an example event from (c). Scale bars represent 500 pA (vertical) and 1 ms (horizontal).

spectrometry[15] to viral diagnosis. While promising, these approaches remain nascent, hinging currently on expensive instrumentation and computationally demanding analyses.

An emerging platform for biomolecular analysis is the solid-state (SS-) nanopore.[16,17] Briefly, a SS-nanopore is composed of a thin, insulating membrane supported by a silicon chip and featuring a single, nanometer-scale pore. When the membrane is used as a partition between reservoirs of electrolyte solution, the application of a voltage bias across it generates an electric field that can facilitate the electrokinetic movement of charged molecules through the opening. Each translocation temporarily interrupts the measured ionic current and results in a signal (or "event") that can be exploited for biosensing and molecular evaluation. SS-nanopores have been employed extensively to identify nucleic acids,[18−20] proteins,[21−23] biological nanoparticles (*e.g.*, exosomes[24]), and synthetic nanoparticles.[25−27] Recently, the platform has also been applied to viral diagnostics with several reports[28−30] describing the detection or analysis of whole virions, including *Paramecium bursaria* Chlorella virus (PBCV-1),[31] Hepatitis B,[32] HIV,[33] and influenza.[34,35] However, probing whole viruses does not explicitly provide a route to viral discrimination without *a priori* knowledge of the pathogens present in a fluid. Consequently, the translational potential of these approaches has been narrow. The alternative approach of detecting specific viral biomarkers has been explored with the platform as well. Recently, Nouri et al.[36] demonstrated the solid-state nanopore detection of specific HIV-1 DNA sequences using a CRISPR-Cas12a approach. Remaining challenges with this approach include potential difficulty in accounting for CRISPR cleavage kinetics and an inability to apply the method directly to HIV genomic RNA. In another example, Niedzwiecki et al.[37] studied nucleocapsid protein 7, a protein constituent specific to HIV, by probing the effect of binding to a synthetic RNA on its translocation dynamics. Moreover, the detection of nucleic acid (sequence-based) viral bioindicators has been challenging with SS-nanopores. This is at least in part because the platform itself lacks intrinsic selectivity; since all passing molecules produce a signal, the differentiation of particular target sequences is difficult.

To address the selectivity gap with conventional SS-nanopore assessment, our group has established an approach to detect and quantify target nucleic acids.[38] Briefly, the two-component assay employs a short nucleic acid fragment (< ~250 bp) featuring a single biotin tag and a small, globular protein (54 kDa monovalent streptavidin,[39,40] or MS). When each is introduced individually to a SS-nanopore of appropriate size (typically ~7.5−11 nm diameter), they do not yield significant events due to their small size and rapid transit time (Figure 1a,b). On the contrary, when bound together to form a nucleoprotein complex, the larger structure interacts sterically with the pore walls to slow the translocation speed and produce translocation events (Figure 1c). We previously extended this basic assay to allow for the detection of nucleic acid sequences[41] by exploiting the observation that events are generated by protein-bound duplex constructs but not single-strands bound to protein. Through the introduction of a biotin-labeled DNA probe to a mixture of single-strand sequences, duplex formation is possible only when antisense molecules are present, yielding the specific detection of target sequences.

However, to date, this detection has been demonstrated only for naturally short, single-strand nucleic acids like microRNAs, for which the probe can be matched in size to the target. In this report, we expand our protocols to enable the SS-nanopore assay to detect conserved sequence motifs within large single-

https://doi.org/10.1021/acsnano.0c10887
ACS Nano XXXX, XXX, XXX−XXX

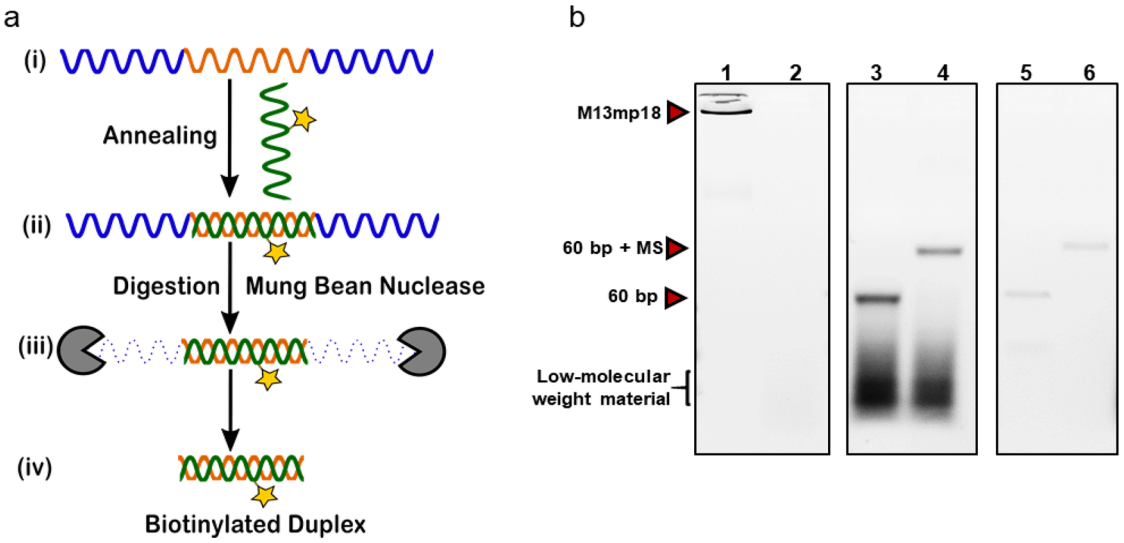

Figure 2. (a) Schematic representation of steps involved in the isolation of subsequences from a single-strand genome. A long genome (i) containing a target sequence motif (orange) is annealed (ii) to a complementary DNA probe (green) tagged with a biotin moiety (star). The resulting construct is subjected to digestion (iii) with a single-strand specific endonuclease (mung bean nuclease or MBN) to yield a monobiotinylated duplex (iv). (b) Agarose gel electrophoresis analysis. Lane 1, M13mp18 DNA alone; lane 2, M13mp18 DNA digested with MBN; lane 3, 60 bp duplex isolated from M13mp18 DNA; lane 4, same as lane 3 bound to MS; lane 5, synthetic biotinylated 60 bp duplex DNA construct; lane 6, same as lane 5 bound to MS. Full gel is shown in Figure S1.

strand genomes, including viral genomes. Our strategy, which involves annealing to a synthetic probe sequence and the subsequent digestion of nontarget regions, yields a short duplex construct capable of binding to MS and consequently being analyzed by our SS-nanopore assay. Like PCR, high specificity is achieved through Watson−Crick base pairing, but our approach provides potential advantages in both time and cost. We validate the technique using a model DNA genome (M13mp18 bacteriophage DNA) and then demonstrate its extension to RNA, the more common carrier of viral genetic information, by probing a conserved sequence in HIV-1B. The ability of our approach to assess target subsequences within large DNAs and RNAs suggests the potential value of SS-nanopores not only for viral identification but also for other nucleic acid detection applications as well.

RESULTS AND DISCUSSIONS

Internal Sequence Isolation. Our general approach to produce biotinylated duplex constructs from single-strand genomes is shown schematically in Figure 2a. First, a short target region is identified within the genome (Figure 2a(i), orange) and used to design a complementary probe construct (Figure 2a(i), green) consisting of a synthetic DNA oligonucleotide with a single biotinylated base. This probe is then mixed with the genomic material and subjected to a single thermal cycle to promote annealing, resulting in constructs that are locally duplex at the target site but single-stranded elsewhere (Figure 2a(ii)). Finally, the constructs are incubated with mung bean nuclease (MBN), an endonuclease that catalyzes the degradation of internal phosphodiester bonds specifically in single-strand nucleic acids.[42] This treatment digests unannealed genomic regions (Figure 2a(iii)) but leaves the target sequence intact, yielding duplex fragments matched in length to the synthetic probe and retaining the biotin tag for downstream analysis (Figure 2a(iv)). Note that the positioning of the biotin near the center of the DNA probe reduces the chance of inadvertent MBN digestion due to thermally driven structural fluctuations (or "breathing") of the duplex product at its ends.

We established our protocol initially using, as a template, a model single-strand DNA genome derived from the bacteriophage M13mp18 (7249 nt in length). For a first demonstration, we employed a 60 nt synthetic biotinylated probe designed with complementarity to an internal motif of M13mp18 (see the Materials and Methods section) and determined assay success through gel analysis. M13mp18 alone yielded a well-defined band in the gel (Figure 2b, lane 1). Upon incubation with MBN (Figure 2b, lane 2), we observed a total loss of features in the lane, confirming the ability of the nuclease to digest the single-strand genomic DNA completely. Repeating the same procedure after annealing the biotinylated 60 nt probe to M13mp18 (Figure 2b, lane 3), we instead observed a distinct band that ran to the same position as a synthetic 60 bp construct (Figure 2b, lane 5), showing that the 60 bp construct was successfully isolated. Some low-molecular weight material was also seen following isolation (Figure 2b, lane 3, bottom), which we attribute to secondary structure elements in the template DNA or probes that would be slower to digest due to their local duplex nature. The subsequent binding of the isolate to MS yielded a shift (Figure 2b, lane 4) identical to that of the synthetic construct (Figure 2b, lane 6), verifying the retention of an active biotin following nuclease treatment. Note that no shift was observed in the low-molecular weight products (Figure 2b, lane 4, bottom), indicating that they were not biotinylated.

MBN incubation time was critical for successful target isolation. When insufficient time or enzyme concentration were used, single-strand overhangs remained at the ends of the products, as indicated by a smeared band on the gel (Figure S2). This could negatively impact downstream processes. Conversely, extended incubation times could induce a loss of observed product (Figure S2b). Even though the specificity of MBN for single-strand DNA is ~30 000× more than that for duplex,[43] deterioration could be driven by breathing at the

https://doi.org/10.1021/acsnano.0c10887
ACS Nano XXXX, XXX, XXX−XXX

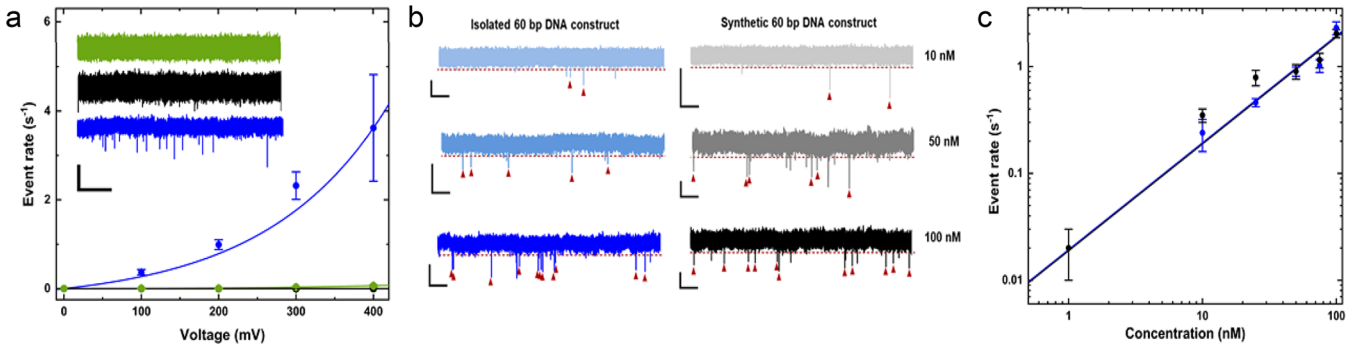

Figure 3. SS-nanopore analysis of 60 bp constructs isolated from M13mp18 DNA. (a) Voltage-dependent translocation event rates for MS alone (400 nM, green), biotinylated 60 bp M13mp18 isolate alone (100 nM, black), and the combination following coincubation (blue). Solid lines are exponential fits to the data. Inset: example current traces for each group (colors matched). (b) Example current traces for different concentrations (10, 50, and 100 nM) of 60 bp isolate (left) and synthetic 60 bp construct (right), each with MS bound. The red dashed line represents threshold amplitude, and each red arrow indicates an identified event. (c) Concentration dependence of event rates for biotinylated 60 bp M13mp18 isolate (blue) and a synthetic biotinylated 60 bp DNA construct (black), each bound to MS. Solid lines are linear fits to the data points. All scale bars represent 250 ms (horizontal) and 500 pA (vertical), and all measurements were performed at 300 mV applied bias. Further analyses shown in Figures S3 and S4.

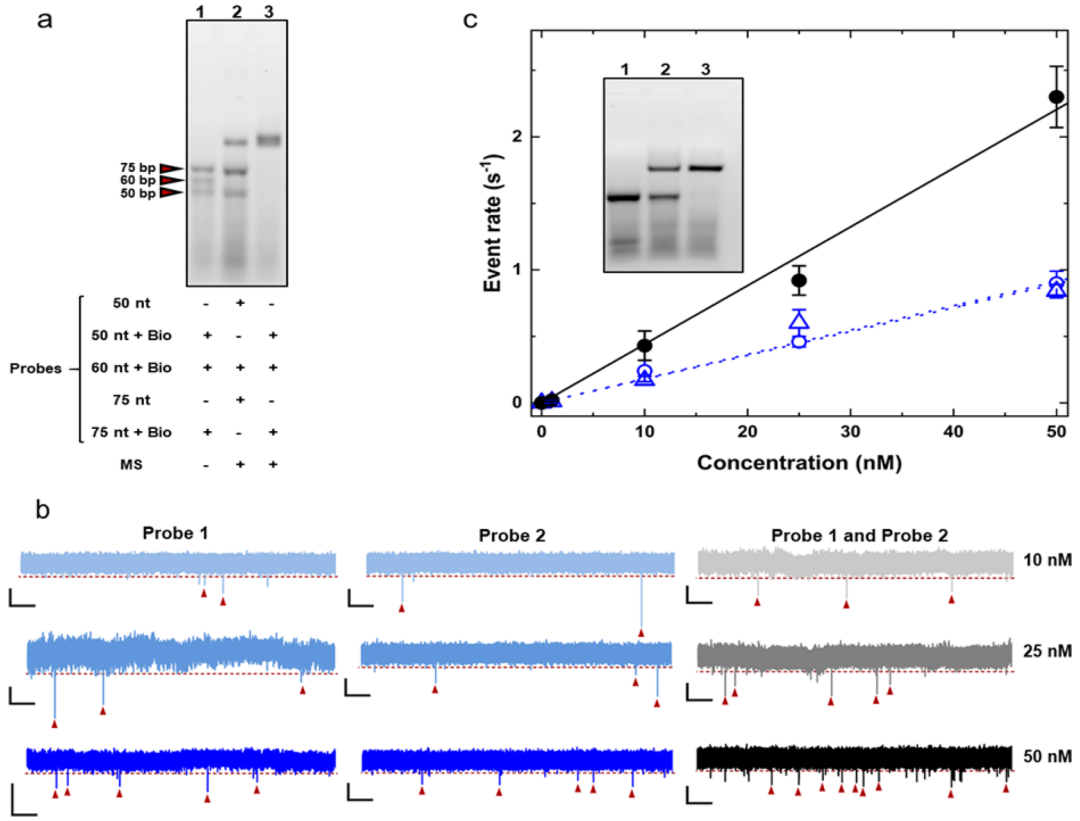

Figure 4. Isolation and analysis of multiple distinct products from a single-strand genome. (a) Gel analysis. Lane 1, isolated products from M13mp18 using three DNA probes (50, 60, and 75 nt); lane 2, electromobility shift assay in the presence of MS when only one probe is biotinylated; lane 3, electromobility shift assay in the presence of MS when all probes are biotinylated. Full gel is shown in Figure S5. (b) Example current traces at multiple concentrations for 60 bp products isolated from M13mp18 using probe 1 and probe 2 both independently (left and center) and together (right) after binding with MS. The red dashed lines represent threshold amplitude, and each red arrow indicates an identified event. All scale bars represent 250 ms (horizontal) and 500 pA (vertical). (c) SS-nanopore assay signal amplification through the use of multiple probes. Concentration-dependent event rates for M13mp18 isolates using two independent biotinylated 60 nt probes separately (blue circles and triangles, respectively) and for products using both 60 nt probes in tandem (black), all measured after binding with MS. Solid lines are linear fit to the data. Inset: agarose gel showing two independent 60 bp duplex isolates where neither are biotinylated (lane 1), one is biotinylated (lane 2), and both are biotinylated (lane 3), each in the presence of MS. The lower band is 60 bp, and the upper band is 60 bp bound to MS. Full gel is shown in Figure S6. All SS-nanopore measurements were performed at 300 mV applied bias. Additional analyses are shown in Figure S7.

ends providing stochastic single-strand recognition points for MBN activity.

SS-Nanopore Detection of Target DNA Motifs. Having demonstrated the successful isolation of a target subsequence

https://doi.org/10.1021/acsnano.0c10887
ACS Nano XXXX, XXX, XXX−XXX

from a large single-strand DNA genome, we next demonstrated the viability of the isolated constructs to be analyzed with our selective SS-nanopore assay. We first performed a series of voltage-dependent measurements of translocation event rates on both the 60 bp product of M13mp18 isolation and MS alone (Figure 3a, black and green). We found that neither produced significant signals up to at least 400 mV. However, when combined, the resulting nucleoprotein construct produced clear events, the rate of which increased exponentially with applied voltage (Figure 3a, blue). These contrasting signals were in agreement with our past measurements using fully synthetic constructs[41,44] and demonstrated our ability to detect a target internal DNA motif using the assay with high selectivity. Indeed, the event rate associated with MS-bound 60 bp isolate was more than an order of magnitude higher than the rates of either constituent alone under all conditions.

We next conducted a concentration-dependent analysis to investigate quantitation with our assay. Using a single applied voltage (300 mV), we first performed a series of measurements on the biotinylated 60 bp M13mp18 product and synthetic 60 bp dsDNA, each bound to MS. Example current traces for both constructs recorded at 300 mV are also shown in Figure 3b. All current traces are represented with their individual scale bars as measurements of translocation event rates that were carried over different nanopores, having different levels of noise. Across a range of 1−100 nM, we observed a linear trend in the measured event rate with a slope of 0.019 ± 0.002 nM^{-1} s^{-1} (Figure 3c, blue). This trend matched our previous results[44] with the same assay and was in quantitative agreement with similar measurements performed on a synthetic biotinylated 60 bp DNA construct bound to MS, which yielded a slope of 0.019 ± 0.001 nM^{-1} s^{-1} (Figure 3c, black). The close correspondence demonstrated that our isolation protocol yielded an intact duplex DNA construct capable of SS-nanopore assay detection and indicated that targets could be quantified directly from the event rate. Considering the low false positive rate (*i.e.*, the number of events associated with control measurements), we found that concentrations as low as 1 nM could be resolved easily without further improvement. Given the low fluid volume used in our system (10 μL), this corresponds to a total of 10 fmoles of product or an equivalent amount of single-strand genomes in solution.

Isolation and Detection of Multiple Target Motifs in a Single Genome. Because MBN is an endonuclease and does not require 3′ or 5′ ends to initiate, it should be possible for single-strand regions between multiple annealed probes along a single template molecule to be digested, thereby yielding multiple discrete products from one genome. To test this approach, we next repeated our isolation protocol with M13mp18 using three distinct synthetic probes. For easy differentiation on a gel, three biotinylated probes with different lengths were utilized: the same 60 nt probe sequence employed above, as well as 50 and 75 nt probes with complementarity to disparate regions of the genomic sequence (see the Materials and Methods section). Implementing an isolation protocol identical to that described above for M13mp18 but including all three probes during the anneal step, we subsequently observed three separate bands on the gel (Figure 4a, lane 1), demonstrating the isolation of discrete products simultaneously. To verify the identities of these bands as the intended target constructs and to confirm the retention of the biotin tags, two versions of the isolation procedure were performed: one in which a biotinylated 60 nt probe and unlabeled 50 and 75 nt probes were used and one in which all three probe lengths were biotinylated. After mixing the resulting products with MS, we observed that only the center band shifted for the product of the first treatment (Figure 4a, lane 2), validating the selectivity of the protocol. For the second treatment, all bands were found to shift (Figure 4a, lane 3), demonstrating consistent retention of the biotin moiety in all cases. The complete gel image with all positive and negative controls is in Figure S5. In principle, this same process could be extended to arbitrary numbers of probes and sizes given sufficient sequence differentiability. For the purpose of quantifying target genomes with our SS-nanopore assay, the simultaneous probing of multiple target sequences could provide a critical route to signal amplification without the need for PCR; when each genome provides multiple sequence targets, the overall sensitivity of detection should be improved concomitantly. We next demonstrated this concept empirically. Because the translocation event rate is known to vary with construct length in our assay,[44] the three probes used above for gel visualization could not be employed effectively here. Instead, we used two biotinylated synthetic probes of the same length (60 nt) that recognized different regions of M13mp18 (see the Materials and Methods section). The biotinylated products of isolation for both probes were first confirmed by gel. When two probes were included in the anneal step, we retrieved a single band at the 60 bp position (Figure 4c, inset lane 1). While the brightness of the observed band suggested qualitatively that more product was generated, the common size of both constructs made deconvolution challenging. To address this, we also performed the same isolation procedure with one biotinylated probe and one unmodified probe. In this case, binding to MS shifted only one of the two products (Figure 4c, inset lane 2), confirming that both target sequences were isolated independently. For completeness, when both probes were biotinylated, both were found to shift to a single position upon MS binding (Figure 4c, inset lane 3), as expected.

We next analyzed these products both separately and in tandem by SS-nanopore. Figure 4b shows example current traces for each isolate independently and in tandem across multiple concentrations. When either 60 nt probe was used individually (Figure 4c, blue circles and triangles), we observed a concentration-dependent event rate that was identical both to previous measurements (see Figure 3c) and to each other, exhibiting slopes of 0.018 ± 0.001 and 0.018 ± 0.002, respectively. However, when both probes were included concurrently, we recorded a dependence that was approximately double that of the single-probe measurements (Figure 4c, black), yielding a slope of 0.044 ± 0.002. This confirmed that signal amplification could indeed be achieved through the use of multiple probes having complementarity to different regions of a single genome. We note that it could in principle be possible to assign events to specific sequence motifs in this approach to achieve multiplexing. However, most routes to differentiation (*e.g.*, different length probes, different number of biotin moieties) would also impact translocation dynamics, precluding the event rate quantification we pursue here.

Detection of RNA Sequence Motifs. We finally extended our approach toward pathogen detection by examining a viral genome. Because single-strand RNA viral genomes are significantly more abundant than single-strand DNA viruses, we chose to apply our protocols and subsequent nanopore analysis to an RNA genome. Here, we focused on HIV,[45] a

https://doi.org/10.1021/acsnano.0c10887
ACS Nano XXXX, XXX, XXX−XXX

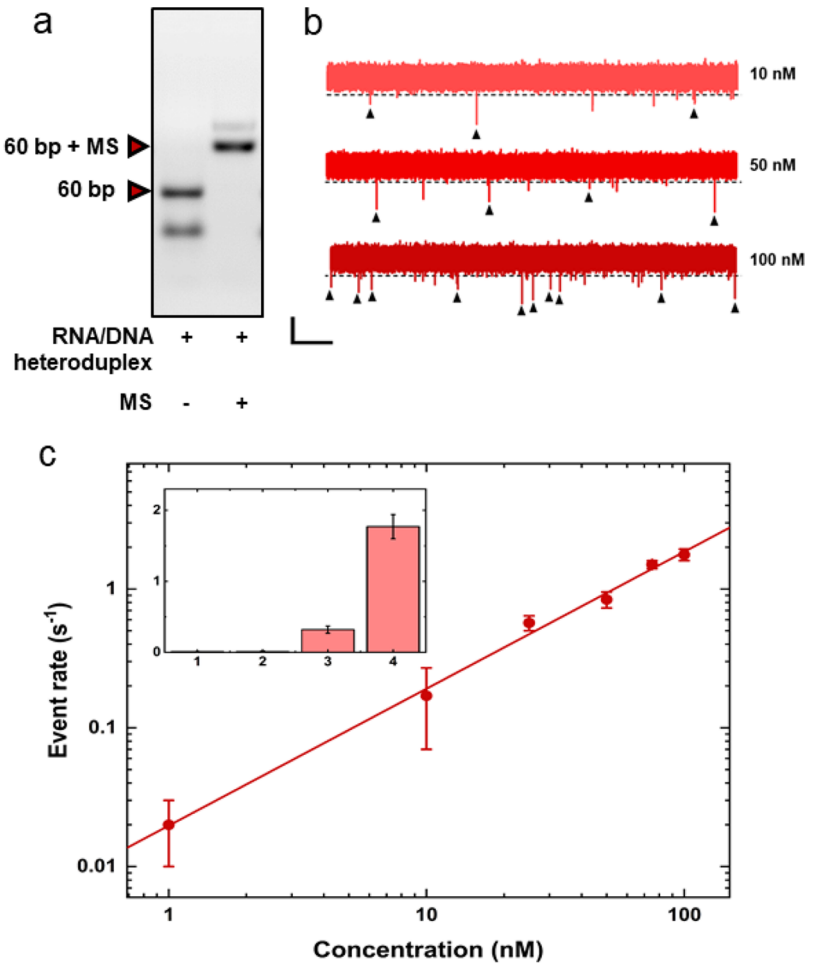

Figure 5. (a) Gel analysis of sequence isolation from full-length HIV-1B RNA. Lane 1, biotinylated 60 bp RNA/DNA heteroduplex isolated from full-length HIV-1B RNA; lane 2, biotinylated 60 bp RNA/DNA heteroduplex isolated from full-length HIV-1B RNA bound to MS. Full gel is shown in Figure S9. (b) Example current traces for RNA/DNA heteroduplex bound to MS measured at three different concentrations. The black dashed lines represent threshold amplitude, and each black arrow indicates an identified event. Scale bars represent 250 ms (horizontal) and 500 pA (vertical). Additional analyses are shown in Figure S10. (c) Concentration-dependent event rate for monobiotinylated 60 bp RNA/DNA heteroduplex isolated from full-length HIV-1B RNA bound to MS. The solid line is a linear fit to the data. Inset: event rates for column 1, HIV-1B isolate alone (100 nM); column 2, MS alone (4 μM); column 3, 60 nt DNA probe bound to MS (100 nM); and column 4, HIV-1B isolate bound MS (100 nM). All measurements were performed at 300 mV applied voltage.

lentivirus (subcategory of retrovirus) consisting of an enveloped single-strand RNA. HIV is categorized into two types: HIV-1 and HIV-2, with the former being a more virulent and major cause of infections globally.[46] For this study, we specifically use as a model the viral genome of HIV-1B, the dominant subtype in the Americas, Western Europe, Australia, and Asia.[47] While our DNA model M13mp18 had a stable, well-documented genome, HIV-1B is known to undergo mutation, making the identification of a highly conserved target sequencing more challenging. We therefore first performed a sequence alignment of ~4300 known variants. From this list, we identified a 60 nt motif in HIV-1B that was more than 90% conserved among all available sequences and designed a complementary biotinylated 60 nt DNA probe for use in our isolation protocol.

As an initial check, we performed an independent test of MBN nuclease on full-length HIV-1B RNA alone because minimally the MBN digestion step of our procedure must degrade all of the template genome. Some of the available literature[42,48] has reported that MBN activity is similar for DNA and RNA substrates, suggesting that our existing approach for isolation from DNA should hold. In contrast, Kole et al.[49] found that esters of ribonucleotides are cleaved by the enzyme 100 times faster than deoxyribonucleotides due to the presence of a 2′-hydroxyl group, suggesting that a significantly lower MBN exposure would be required for an RNA genome. To test this directly, we performed a titration series of HIV-1B RNA against MBN (Figure S8) and found a sufficient level of degradation for the same incubation time as M13mp18 DNA but with a 400-fold lower concentration.

Taking this difference into account, we performed the full isolation protocol after annealing full-length HIV-1B RNA with the biotinylated 60 nt probe and observed an efficient recovery of the heteroduplex (RNA−DNA hybrid) product (Figure 5a, lane 1). As above, binding of the product with MS yielded an electromobility shift in gel analysis (Figure 5a, lane 2) that matched the behavior of a synthetic biotinylated DNA duplex, as shown in Figure S9 and confirming the presence of the biotin in the final constructs. We also observed an additional band below the 60 bp product. In contrast with the low-molecular weight smear observed in Figure 2b (lanes 3−4), this band shifted with MS incubation, identifying it as an

https://doi.org/10.1021/acsnano.0c10887
ACS Nano XXXX, XXX, XXX−XXX

unconjugated biotinylated DNA probe. This is not unexpected; because of the strong reduction in MBN concentration used here, single-strand probes that were digested by the nuclease under DNA conditions were left largely intact. However, because single-strand nucleic acids do not contribute to the SS-nanopore signal even when bound to MS,[43] their presence was not consequential to subsequent analyses.

To demonstrate the viability of our overall approach for RNA analysis, we finally conducted our SS-nanopore assay with the HIV-1B isolate. Figure 5c shows the result of concentration-dependent event rate measurements using the biotinylated heteroduplex product. We again found a linear relationship exhibiting a slope of 0.018 ± 0.001. This result demonstrated excellent consistency with our measurements on M13mp18 above (*c.f.*, Figure 3c), indicating that the sensitivity for RNA genomes should be identical to that of DNA genomes. As an additional control, we also measured the biotinylated 60 nt single-strand DNA probe bound to MS at a a very high concentration (100 nM) and found that even that extreme amount yielded an event rate about an order of magnitude less than that of the duplex construct (Figure 5c, inset). This confirmed that the undigested probe remaining after isolation from HIV-1B did not impact the measurement significantly. Example current traces corresponding to control measurements (HIV-1B isolate, MS, and 60 nt probe bound to MS) are shown in Figure S11.

CONCLUSION

In this study, we have reported an approach for the isolation of sequence motifs from single-strand genomes and their subsequent detection using a selective SS-nanopore assay. For isolation, a synthetic, biotinylated DNA oligonucleotide probe was designed with complementarity to a known sequence in the target genome. After annealing, the unpaired portions of the genomic template were digested using a single-strand specific endonuclease, resulting in duplex constructs matched in length to the probe. Because of the incorporated biotin moiety, these duplexes were amenable to analysis with a SS-nanopore assay in which the presence of a bound MS protein enables selective detection. We first demonstrated the approach using as a model the single-strand bacteriophage DNA M13mp18, showing quantitative assessment of a single motif and extending to multiple independent sequence motifs in a common genome. We then applied the same concept to human pathogen detection by probing the HIV-1B genome. After adapting our protocols to work with RNA, we isolated a highly conserved sequence from the genome and observed similar results as with the DNA target, showing an ability to sense as little as 10 femtomoles of motif (and thus HIV-1B genomes) using only a single probe sequence.

Our method offers potential advantages over standard methods like PCR; while both are quantitative, SS-nanopore analysis is all-electronic (*i.e.*, more cost-effective than optical readouts) and could offer faster time-to-answer as it explicitly does not require enzymatic amplification and the thermal cycling it entails. In addition, because we are able to probe RNA directly, our process does not require reverse transcription into cDNA prior to analysis. Ultimately, our results expand the capabilities of the approach and its associated protocols beyond the detection and quantification of short, size-matched targets like microRNA[41] to include any single-strand targets. This will enable numerous additional applications including the pathogen screening of viral genomes, phylogeny and taxonomy assessments using rRNA, and transcriptional analysis of mRNA.

MATERIALS AND METHODS

Biomolecules. All synthetic oligonucleotides, including all synthetic probes and complementary sequences used to form control constructs, were obtained commercially (Integrated DNA Technologies, Coralville, IA). The sequences of all probes are listed in Table S1. All the oligonucleotides were resuspended in deionized water free of DNase and RNase (Invitrogen, Grand Island, NY) to a stock concentration of 200 μM and stored at −20 °C before use. Single-strand M13mp18 DNA was obtained commercially (New England Biolabs, Ipswich, MA). Synthetic duplex constructs were formed by annealing complementary oligonucleotides at a molar ratio of 1:1, heating to 95 °C for 10 min, and slowly cooling to room temperature. For all MS binding reactions, constructs were reacted with MS at a concentration equal to the biotinylated probe concentration in 1X PBS for 10 min at room temperature.

HIV-1 BH10 noninfectious molecular clone (pBH10)[50] was obtained from the NIH AIDS Reagent program (catalog #90) and subcloned into the SstI site of SP64 vector (Promega, Madison, WI) as a competent bacterial culture that was stored in glycerol stock at −80 °C prior to use. Fifty microliters of bacterial stock was plated on an LB agar plate with a 50 μg/mL concentration of ampicillin and grown overnight in a bacterial incubator at 37 °C. Formed colonies were isolated, transferred to 5 mL of LB with 5 μL of 10 mg/mL ampicillin, and then put in a shaker (135 rpm) at 37 °C for 12−16 h until reaching an optical density (A_{600}) between 2 and 4. The bacterial culture was spun down at 5000*g* at 4 °C for 20 min to form a bacterial pellet that was isolated and used as a source for plasmid DNA using a Wizard SV Mini Prep plasmid DNA purification kit (Promega). One microgram of the purified pBH10 plasmid was mixed with 1 U of NheI (New England Biolabs) and 3 μL of 10X NEBuffer 3.1 (New England Biolabs) in a 30 μL aliquot and incubated at 37 °C for 1 h to cut the DNA downstream of the SP6 promoter and BH10 insert. After heat inactivating the NheI at 70 °C, a small aliquot of the product was analyzed on a 1% agarose gel to ensure successful linearization. The linearized DNA was then processed with a HiScribe SP6 RNA synthesis kit (New England Biolabs) to synthesize full-length viral RNA product following the manufacturer's suggested protocol. One microliter of SUPERase•In RNase inhibitor (Invitrogen) was added prior to sample storage at −20 °C for stability. For all RNA processing steps, nuclease-free reagents were employed and work was carried out in an Airclean PCR workstation (AirClean Systems, Creedmore, NC) to reduce contamination.

DNA Sequence Isolation Protocol. Annealing was carried out by mixing synthetic probes and M13mp18 DNA at a molar ratio of 13:1 in water, heating to 95 °C for 10 min, and then slowly cooling to room temperature. The digestion of unconjugated regions of M13mp18 and the excess probes was performed by adding 20 U MBN (New England Biolabs) for every 2.5 μg of M13mp18, adding 10X MBN reaction buffer (New England Biolabs) to reach a final concentration of 1X, and incubating the mixture at 30 °C for 15 min. Endonuclease activity was quenched by adding an equal volume of phenol/chloroform/isoamyl alcohol (25:24:1) (Acros Organics, Morris, NJ) followed by centrifugation at 17 000*g* in phase lock gel tubes (Quantabio, Beverly, MA). The process was repeated once using pure chloroform to remove any residual phenol. The aqueous component containing DNA isolate was retrieved and further purified using a nucleotide purification kit (Qiagen, Germantown, MD). Obtained DNA constructs were redispersed in DNase-/RNase-free water at a final concentration of 320 nM and diluted as needed for concentration-dependent studies. The samples were loaded on 3% agarose gel in 1X TBE buffer with Gel Red nucleic acid dye (Phenix Research Products, Candler, NC) and imaged by E-Gel Imager system (Invitrogen, Carlsbad, CA) to confirm products.

RNA Sequence Isolation Protocol. The multiple sequence alignment program Kalign[51] (European Informatics Center) was used to align sequences of HIV-1B for identifying a candidate probe.

https://doi.org/10.1021/acsnano.0c10887
ACS Nano XXXX, XXX, XXX−XXX

Full genome sequences (4300) of HIV-1B retrieved from Los Alamos National Laboratory (LANL) database[52] were considered ranging in collection year and geographical area to maximize the precision of the conserved sequence. The target conserved motif was selected from candidate sequences with more than 90% alignment among all considered genomes. Annealing was performed using the same conditions as employed for M13mp18 but with a molar ratio of probe to RNA of 40:1. The necessity of this higher ratio as compared to the DNA target was determined empirically as shown in Figure S12. Magnesium chloride was added to the annealing mixture at a final concentration of 200 μM to enhance the stability of the duplex by screening the negatively charged phosphate backbones of the nucleic acids. After annealing, 0.2 U of MBN was added for every 10 μg of RNA, 10X MBN reaction buffer was added to reach a final concentration of 1X, and the mixture was incubated for 15 min at 30 °C. All other steps were followed as for M13mp18 above except that the use of the nucleotide removal kit for purification was replaced with an ethanol precipitation step to reduce contamination from spin columns and buffers. The obtained heteroduplex products were redispersed in DNase-/RNase-free water at a final concentration of 320 nM and diluted as needed for concentration-dependent measurements. Products were analyzed by gel electrophoresis as with M13mp18 as above but with the electrophoretic cells cleaned using a 0.1% SDS solution in 70% ethanol before gel casting.

Solid-State Nanopores. Silicon chips with a 4 × 4 mm^2 frame size and supporting a 20 μm silicon nitride window were obtained commercially (Norcada, Alberta, Canada). RNA measurements (see Figure 5b,c) were performed on devices with 30 nm thick membranes, while all other measurements shown used 20 nm thick membranes. In each membrane chip, a single nanopore 7.5−11 nm in diameter was fabricated using a scanning helium ion microscope (Orion PLUS, Carl Zeiss, Peabody, MA) technique described elsewhere[53] and stored in 50% ethanol prior to use. Directly before a measurement, chips were rinsed with ethanol and HPLC grade water, dried under filtered air flow, and cleaned with air plasma (30W) for 2 min on each side to promote hydrophilicity. The silicon chip was then placed into a custom 3D printed flow cell, and measurement buffer (900 mM NaCl, 0.5X PBS) was introduced immediately on both sides. For the application of voltage and the measurement of current, Ag/AgCl electrodes were immersed into the solution on each side and connected to a patch-clamp amplifier (Axopatch 200B, Molecular Devices, San Jose, CA). Pore diameters were verified through the analysis of a linear current−voltage curve and a comparison to a standard model.[54] Translocation measurements were carried out by replacing the measurement buffer in the *cis* chamber with analyte in measurement buffer. All current traces were collected at a bandwidth of 200 kHz with a 100 kHz four-pole Bessel filter and analyzed using custom software through which an additional 30 kHz low-pass filter was applied. Event rates were determined by analyzing discrete 3.2 s blocks of data to identify events as defined by signals exceeding a threshold amplitude of 4.5σ and having a duration between 12.5 μs and 2 ms.

ASSOCIATED CONTENT

Supporting Information

The Supporting Information is available free of charge at https://pubs.acs.org/doi/10.1021/acsnano.0c10887.

Figures of gel analyses, dwell time vs conductance change scatter plots with accompanying histograms, and example control current traces and table of probe sequences (PDF)

AUTHOR INFORMATION

Corresponding Author

Adam R. Hall − *Virginia Tech-Wake Forest University School of Biomedical Engineering and Sciences, Wake Forest School of Medicine, Winston-Salem, North Carolina 27101, United States; Comprehensive Cancer Center, Wake Forest School of Medicine, Winston-Salem, North Carolina 27157, United States;* orcid.org/0000-0003-2053-6075; Email: arhall@wakehealth.edu

Authors

Komal Sethi − *Virginia Tech-Wake Forest University School of Biomedical Engineering and Sciences, Wake Forest School of Medicine, Winston-Salem, North Carolina 27101, United States*

Gabrielle P. Dailey − *Department of Chemistry and Biochemistry, University of North Carolina at Greensboro, Greensboro, North Carolina 27402, United States*

Osama K. Zahid − *Virginia Tech-Wake Forest University School of Biomedical Engineering and Sciences, Wake Forest School of Medicine, Winston-Salem, North Carolina 27101, United States*

Ethan W. Taylor − *Department of Chemistry and Biochemistry, University of North Carolina at Greensboro, Greensboro, North Carolina 27402, United States*

Jan A. Ruzicka − *Department of Basic Pharmaceutical Sciences, Fred Wilson School of Pharmacy, High Point University, High Point, North Carolina 27268, United States*

Complete contact information is available at: https://pubs.acs.org/10.1021/acsnano.0c10887

Notes

The authors declare the following competing financial interest(s): A.R.H. is listed as inventor on a patent covering the SS-nanopore assay. The other authors declare no competing interests.

ACKNOWLEDGMENTS

The authors gratefully acknowledge the Howarth Lab (Oxford University) for supplying MS proteins. The following reagent was obtained through the NIH AIDS Reagent Program, Division of AIDS, NIAID, NIH: HIV-1 BH10 Noninfectious Molecular Clone (pBH10) from Dr. Beatrice Hahn and Dr. George Shaw (cat# 90). This project was supported by NIH award R33CA246448 and by the Wake Forest Technology Development Program through a Catalyst Phase II award, both to A.R.H.

REFERENCES

(1) Oldstone, M. B. A. History of Virology. In *Encyclopedia of Microbiology*; Schmidt, T. M., Ed.; Academic Press: Cambridge, MA, 2014; pp 608−612.

(2) Woolhouse, M.; Scott, F.; Hudson, Z.; Howey, R.; Chase-Topping, M. Human Viruses: Discovery and Emergence. *Philos. Trans. R. Soc., B* **2012**, *367*, 2864−2871.

(3) Rosenberg, R. Detecting the Emergence of Novel, Zoonotic Viruses Pathogenic to Humans. *Cell. Mol. Life Sci.* **2015**, *72*, 1115−1125.

(4) Woolhouse, M.; Gaunt, E. Ecological Origins of Novel Human Pathogens. *Crit. Rev. Microbiol.* **2007**, *33*, 231−242.

(5) Sudhan, S. S.; Sharma, P. Human Viruses: Emergence and Evolution. In *Emerging and Reemerging Viral Pathogens*; Ennaji, M. M., Ed.; Academic Press: Cambridge, MA, 2020; pp 53−68.

(6) Kiselev, D.; Matsvay, A.; Abramov, I.; Dedkov, V.; Shipulin, G.; Khafizov, K. Current Trends in Diagnostics of Viral Infections of Unknown Etiology. *Viruses* **2020**, *12*, 211.

(7) Harapan, H.; Itoh, N.; Yufika, A.; Winardi, W.; Keam, S.; Te, H.; Megawati, D.; Hayati, Z.; Wagner, A. L.; Mudatsir, M. Coronavirus

Disease 2019 (COVID-19): A Literature Review. *J. Infect. Public Health* **2020**, *13*, 667−673.
(8) Mackay, I. M.; Arden, K. E.; Nitsche, A. Real-Time PCR in Virology. *Nucleic Acids Res.* **2002**, *30*, 1292−1305.
(9) Green, T. A.; Black, C. M.; Johnson, R. E. Evaluation of Bias in Diagnostic-Test Sensitivity and Specificity Estimates Computed by Discrepant Analysis. *J. Clin. Microbiol.* **1998**, *36*, 375−381.
(10) Fredricks, D. N.; Relman, D. A. Application of Polymerase Chain Reaction to the Diagnosis of Infectious Diseases. *Clin. Infect. Dis.* **1999**, *29* (3), 475−486 quiz 487−488..
(11) Yang, S.; Rothman, R. E. PCR-Based Diagnostics for Infectious Diseases: Uses, Limitations, and Future Applications in Acute-Care Settings. *Lancet Infect. Dis.* **2004**, *4*, 337−348.
(12) Storch, G. A. Diagnostic Virology. *Clin. Infect. Dis.* **2000**, *31*, 739−751.
(13) Dwenger, A. Radioimmunoassay: An Overview. *J. Clin. Chem. Clin. Biochem.* **1984**, *22* (12), 883−894.
(14) Sun, Q.; Zhao, G.; Dou, W. Blue Silica Nanoparticle-Based Colorimetric Immunoassay for Detection of Salmonella Pullorum. *Anal. Methods* **2015**, *7*, 8647−8654.
(15) Hoofnagle, A. N.; Wener, M. H. The Fundamental Flaws of Immunoassays and Potential Solutions Using Tandem Mass Spectrometry. *J. Immunol. Methods* **2009**, *347*, 3−11.
(16) Dekker, C. Solid-State Nanopores. *Nat. Nanotechnol.* **2007**, *2*, 209−215.
(17) Wanunu, M. Nanopores: A Journey towards DNA Sequencing. *Phys. Life Rev.* **2012**, *9*, 125−158.
(18) Li, J. L.; Gershow, M.; Stein, D.; Brandin, E.; Golovchenko, J. A. DNA Molecules and Configurations in a Solid-State Nanopore Microscope. *Nat. Mater.* **2003**, *2*, 611−615.
(19) Storm, A. J.; Chen, J. H.; Zandbergen, H. W.; Dekker, C. Translocation of Double-Strand DNA through a Silicon Oxide Nanopore. *Phys. Rev. E Stat. Nonlin. Soft Matter Phys.* **2005**, *71*, 051903.
(20) Skinner, G. M.; van den Hout, M.; Broekmans, O.; Dekker, C.; Dekker, N. H. Distinguishing Single- and Double-Stranded Nucleic Acid Molecules Using Solid-State Nanopores. *Nano Lett.* **2009**, *9*, 2953−2960.
(21) Fologea, D.; Ledden, B.; McNabb, D. S.; Li, J. Electrical Characterization of Protein Molecules by a Solid-State Nanopore. *Appl. Phys. Lett.* **2007**, *91*, 053901.
(22) Plesa, C.; Kowalczyk, S. W.; Zinsmeester, R.; Grosberg, A. Y.; Rabin, Y.; Dekker, C. Fast Translocation of Proteins through Solid State Nanopores. *Nano Lett.* **2013**, *13*, 658−663.
(23) Larkin, J.; Henley, R. Y.; Muthukumar, M.; Rosenstein, J. K.; Wanunu, M. High-Bandwidth Protein Analysis Using Solid-State Nanopores. *Biophys. J.* **2014**, *106*, 696−704.
(24) Anderson, W.; Lane, R.; Korbie, D.; Trau, M. Observations of Tunable Resistive Pulse Sensing for Exosome Analysis: Improving System Sensitivity and Stability. *Langmuir* **2015**, *31*, 6577−6587.
(25) Prabhu, A. S.; Jubery, T. Z. N.; Freedman, K. J.; Mulero, R.; Dutta, P.; Kim, M. J. Chemically Modified Solid State Nanopores for High Throughput Nanoparticle Separation. *J. Phys.: Condens. Matter* **2010**, *22* (45), 454107.
(26) Bacri, L.; Oukhaled, A. G.; Schiedt, B.; Patriarche, G.; Bourhis, E.; Gierak, J.; Pelta, J.; Auvray, L. Dynamics of Colloids in Single Solid-State Nanopores. *J. Phys. Chem. B* **2011**, *115*, 2890−2898.
(27) Hall, A. R.; Keegstra, J. M.; Duch, M. C.; Hersam, M. C.; Dekker, C. Translocation of Single-Wall Carbon Nanotubes through Solid-State Nanopores. *Nano Lett.* **2011**, *11*, 2446−2450.
(28) Arjmandi, N.; Van Roy, W.; Lagae, L. Measuring Mass of Nanoparticles and Viruses in Liquids with Nanometer-Scale Pores. *Anal. Chem.* **2014**, *86*, 4637−4641.
(29) McMullen, A.; de Haan, H. W.; Tang, J. X.; Stein, D. Stiff Filamentous Virus Translocations through Solid-State Nanopores. *Nat. Commun.* **2014**, *5*, 4171.
(30) Yang, L.; Yamamoto, T. Quantification of Virus Particles Using Nanopore-Based Resistive-Pulse Sensing Techniques. *Front. Microbiol.* **2016**, *7*, 1500.
(31) Uram, J. D.; Ke, K.; Hunt, A. J.; Mayer, M. Submicrometer Pore-Based Characterization and Quantification of Antibody-Virus Interactions. *Small* **2006**, *2*, 967−972.
(32) Zhou, K.; Li, L.; Tan, Z.; Zlotnick, A.; Jacobson, S. C. Characterization of Hepatitis B Virus Capsids by Resistive-Pulse Sensing. *J. Am. Chem. Soc.* **2011**, *133*, 1618−1621.
(33) Darvish, A.; Lee, J. S.; Peng, B.; Saharia, J.; VenkatKalyana Sundaram, R.; Goyal, G.; Bandara, N.; Ahn, C. W.; Kim, J.; Dutta, P.; Chaiken, I.; Kim, M. J. Mechanical Characterization of HIV-1 with a Solid-State Nanopore Sensor. *Electrophoresis* **2019**, *40*, 776−783.
(34) Arima, A.; Tsutsui, M.; Harlisa, I. H.; Yoshida, T.; Tanaka, M.; Yokota, K.; Tonomura, W.; Taniguchi, M.; Okochi, M.; Washio, T.; Kawai, T. Selective Detections of Single-Viruses Using Solid-State Nanopores. *Sci. Rep.* **2018**, *8*, 16305.
(35) Arima, A.; Harlisa, I. H.; Yoshida, T.; Tsutsui, M.; Tanaka, M.; Yokota, K.; Tonomura, W.; Yasuda, J.; Taniguchi, M.; Washio, T.; Okochi, M.; Kawai, T. Identifying Single Viruses Using Biorecognition Solid-State Nanopores. *J. Am. Chem. Soc.* **2018**, *140*, 16834−16841.
(36) Nouri, R.; Jiang, Y.; Lian, X. L.; Guan, W. Sequence-Specific Recognition of HIV-1 DNA with Solid-State CRISPR-Cas12a-Assisted Nanopores (SCAN). *ACS Sens.* **2020**, *5*, 1273−1280.
(37) Niedzwiecki, D. J.; Iyer, R.; Borer, P. N.; Movileanu, L. Sampling a Biomarker of the Human Immunodeficiency Virus across a Synthetic Nanopore. *ACS Nano* **2013**, *7*, 3341−3350.
(38) Carlsen, A. T.; Zahid, O. K.; Ruzicka, J. A.; Taylor, E. W.; Hall, A. R. Selective Detection and Quantification of Modified DNA with Solid-State Nanopores. *Nano Lett.* **2014**, *14*, 5488−5492.
(39) Howarth, M.; Chinnapen, D. J. F.; Gerrow, K.; Dorrestein, P. C.; Grandy, M. R.; Kelleher, N. L.; El-Husseini, A.; Ting, A. Y. A Monovalent Streptavidin with a Single Femtomolar Biotin Binding Site. *Nat. Methods* **2006**, *3*, 267−273.
(40) Fairhead, M.; Krndija, D.; Lowe, E. D.; Howarth, M. Plug-and-Play Pairing *via* Defined Divalent Streptavidins. *J. Mol. Biol.* **2014**, *426*, 199−214.
(41) Zahid, O. K.; Wang, F.; Ruzicka, J. A.; Taylor, E. W.; Hall, A. R. Sequence-Specific Recognition of MicroRNAs and Other Short Nucleic Acids with Solid-State Nanopores. *Nano Lett.* **2016**, *16*, 2033−2039.
(42) Desai, N. A.; Shankar, V. Single-Strand-Specific Nucleases. *FEMS Microbiol. Rev.* **2003**, *26*, 457−491.
(43) Ardelt, W.; Laskowski, M. Mung Bean Nuclease I. IV. An Improved Method of Preparation. *Biochem. Biophys. Res. Commun.* **1971**, *44*, 1205−1211.
(44) Zahid, O. K.; Zhao, B. S.; He, C.; Hall, A. R. Quantifying Mammalian Genomic DNA Hydroxymethylcytosine Content Using Solid-State Nanopores. *Sci. Rep.* **2016**, *6*, 29565.
(45) Fauci, A. The Human Immunodeficiency Virus - Infectivity and Mechanisms of Pathogenesis. *Science* **1988**, *239*, 617−622.
(46) Nyamweya, S.; Hegedus, A.; Jaye, A.; Rowland-Jones, S.; Flanagan, K. L.; Macallan, D. C. Comparing HIV-1 and HIV-2 Infection: Lessons for Viral Immunopathogenesis. *Rev. Med. Virol.* **2013**, *23*, 221−240.
(47) Junqueira, D. M.; Almeida, S. E. d. M. HIV-1 Subtype B: Traces of a Pandemic. *Virology* **2016**, *495*, 173−184.
(48) Laskowski, M. Purification and Properties of the Mung Bean Nuclease. *Methods Enzymol.* **1980**, *65*, 263−276.
(49) Kole, R.; Sierakowska, H.; Szemplińska, H.; Shugar, D. Mung Bean Nuclease: Mode of Action and Specificity *vs.* Synthetic Esters of 3′-Nucleotides. *Nucleic Acids Res.* **1974**, *1*, 699−706.
(50) Hahn, B. H.; Shaw, G. M.; Arya, S. K.; Popovic, M.; Gallo, R. C.; Wong-Staal, F. Molecular Cloning and Characterization of the HTLV-III Virus Associated with AIDS. *Nature* **1984**, *312*, 166−169.
(51) Lassmann, T.; Frings, O.; Sonnhammer, E. L. L. Kalign2: High-Performance Multiple Alignment of Protein and Nucleotide Sequences Allowing External Features. *Nucleic Acids Res.* **2009**, *37*, 858−865.
(52) Los Alamos National Laboratory. HIV Sequence Database. https://www.hiv.lanl.gov (accessed 2020-08-22).

https://doi.org/10.1021/acsnano.0c10887
ACS Nano XXXX, XXX, XXX−XXX

(53) Yang, J.; Ferranti, D. C.; Stern, L. A.; Sanford, C. A.; Huang, J.; Ren, Z.; Qin, L.-C.; Hall, A. R. Rapid and Precise Scanning Helium Ion Microscope Milling of Solid-State Nanopores for Biomolecule Detection. *Nanotechnology* **2011**, *22*, 285310.
(54) Wanunu, M.; Dadosh, T.; Ray, V.; Jin, J.; McReynolds, L.; Drndic, M. Rapid Electronic Detection of Probe-Specific MicroRNAs Using Thin Nanopore Sensors. *Nat. Nanotechnol.* **2010**, *5*, 807−814.

https://doi.org/10.1021/acsnano.0c10887
ACS Nano XXXX, XXX, XXX−XXX